J. Mechanics in Medicine and Biology

(World Scientific, Singapore/USA)

ISSN (print): 0219-5194 | ISSN (online): 1793-6810

Accepted April 6th 2023.

Computation of Three-Dimensional Blood Flow Development in a 180^O Curved Tube Geometry

Cheng-Hsien Chiang* Rui-Hung Kao**, Tin-Kan Hung***++ and O. Anwar Bég****

*Department of Biomedical Engineering, National Cheng Kung University, Tainan 70101, Taiwan

**Department of Aeronautics and Astronautics, National Cheng Kung University, Tainan 70101, Taiwan.

***Bioengineering and Civil Engineering, University of Pittsburgh, Pittsburgh, PA 15260, U.S.A.

**** MPESG, Department of Aeronautical and Mechanical Engineering, SEE, Salford University, UK.
++ *Corresponding author: Tin-Kan Hung; tkhung@pitt.edu*

Abstract

Computational blood flow studies are providing an increasingly important compliment to clinical experiments in 21st century biomedical engineering. Motivated by probing deeper into this topic, a theoretical and numerical study is presented of the flow induced by an impulsive acceleration to steady state hemodynamics in a curved tube is investigated as a boundary layer developing with time from the curved entrance to a straight tube (blood vessel). The transient processes are simulated with a finite volume method solution of the Navier-Stokes equations. The rapid growth of the boundary layer with the core flow is captured in the curved entrance, along the tube to an axisymmetric flow in the downstream. Secondary flow patterns, centrifugal pressures and total head contours are correlated with longitudinal velocity distributions across various sections. It is observed that the entrance zone is controlled by uniform inlet velocity and centrifugal forces. The high pressure drop in the onset flow is associated with strong acceleration which is comparable to generating systolic pressures. The simulations further indicate that a sustained increment in volumetric flow rate is necessary to maintain the pressure wave in the aorta. Furthermore, the velocity distributions are shown to approach Hagen-Poiseuille flow in the downstream zone. The complex hemodynamic characteristics are visualized effectively with computational simulations and the study demonstrates the excellent ability of this approach in elaborating critical flow details in aortic hemodynamics.

Keywords: *Aortic hemodynamics; numerical; finite volume method; curved tube; boundary layers; secondary flow; centrifugal forces.*

1.Introduction

Analyses of the flow in curved tubes is of fundamental interest for blood transport in arteries and medical devices in addition to other applications including environmental engineering and pipeline hydraulics. The kinematic, dynamic and energy characteristics of such flows have been confirmed to depend on various geometrical and dynamic parameters. In his 1928 analysis of creeping flow, Dean [1] was the first to identify that a pair of counter-rotating secondary vortices are generated along with higher velocities near the outer bend of a coiled tube. Taylor [2] in 1929 further suggested that centrifugal pressures could maintain laminar flow to higher Reynolds number (**Re**). Longitudinal velocity distribution across a curve tube was measured by Barua [3] in 1963 for **Re** = 3930. Steady laminar flows in curve tubes were lucidly reviewed in 1983 by Berger *et al.* [4] who emphasized Dean vortex synthesis and boundary layer development characteristics. Shear stress effects on endothelial changes in steady flow were examined in 1968 by Fry [5]. Fluid dynamic effects on endothelial cells subsequently emerged as important topics in cellular biomechanics. Numerical solutions of flow in rigid and distensible curve tubes were comprehensively investigated by Hung et al.[6] in 1989 using a robust finite difference method which was based on mapping time-dependent meshes onto fixed ones. Hung et al [7] further scrutinized hemodynamics in curved conduits and identified the displacement in peak shear stresses from the inner to the outer wall in pulsating flow. However only limited visualizations were possible at that time due to computational hardware restrictions. With the massive improvements in modern computer and software, the present study aims to obtain more refined solutions associated with the influence of an impulsive acceleration to steady blood flow in an 180^{O} curved tube. Similar laminar flow development in a rotating annular tube [8] was reported in 1973 where spiral structures were examined. This early investigation however was confined to a much lower Reynolds number which did not require enormous mesh densities. The onset acceleration in a human aorta is considered for the present study although the flow rate is not time-dependent and the mean value for the cardiac cycle is adopted. The rapidly varied flow is depicted by velocity contours across various sections from the onset acceleration stage to the steady state. The computations successfully capture the secondary flow patterns, pressure contours, and total heads enabling a comprehensive analysis of 3D boundary layer development with the core flow along the curve to straight tube.

2.Fundamental Equations and Numerical Approach

To investigate the 3D viscous flow development, the arbitrary Lagrangian-Eulerian (ALE) formulation of the Navier-Stokes equations developed by Hirt *et al*.[9] is employed. The integral form of the continuity equation for a volume V bounded by surface S is expressed in vectorial form as follows:

$$\frac{\partial}{\partial t}\int_V \rho dV + \int_S \rho\left(\vec{v} - \vec{v}_b\right)\cdot\vec{n}dS = 0 \tag{1}$$

where $\vec{v}$ is the velocity vector, $\vec{v}_b$ the velocity of the boundary, $\vec{n}$ the unit normal vector, t denotes time, and ρ is blood density. The integral momentum equation is formulated as:

$$\int_V \frac{\partial}{\partial t}\left(\rho\vec{v}\right)dV + \int_S \rho\vec{v}\left(\vec{v} - \vec{v}_b\right)\cdot\vec{n}dS = -\int_S p\mathbf{I}\cdot\vec{n}dS + \int_S \boldsymbol{\tau}\cdot\vec{n}dS \tag{2}$$

Here p is the pressure, $\boldsymbol{I}$ the unit tensor and $\boldsymbol{\tau}$ the viscous stress tensor. Blood flowing in large arteries can be considered as a homogeneous Newtonian fluid. Rheological effects can therefore be neglected since these are generally only critical in smaller arteries. For a tube diameter D of 3.6 cm, the radius of curvature of the 180^{O} bend considered is *1.32D* and the centerline length *11D*. A hyperbolic tangent is used to provide very refined meshes near the wall for adequate resolution in the boundary layer simulation. There are 27 meshes from the center to the wall and 2704 elements on each section. Appropriate no-slip boundary conditions are imposed on the conduit interior wall. The tube is modeled at 274 sections and the mesh comprises a total of 667,888 elements ("finite volumes"). The grid generation has been conducted using ESI CFD-RC GEOM (Alabama, USA). The software ESI CFD-ACE plus has been employed and all computations are executed on a laptop (XPS 15, Dell, USA). The convergence criteria are comfortably controlled and careful monitoring of the same flow rate across each section is performed. The compilation time for computing the flow development from rest (t = 0) to t = 6.9s is approximately 56 hours.

3.Computational Results and Discussions

The computational simulation is produced by an inlet velocity V which is linearly increased to 14 cm/sec in 0.01 second. The acceleration is comparable to an onset systole in the human aorta although the flow rate is kept constant thereafter to study boundary layer development at Reynolds number, **Re =** 1476. **Figure 1 (a)** presents pressure (Pascals) on the symmetric plane at the onset acceleration (t = *0.01 s*). Each curve exceeds the reference pressure P_O at the end-section G-G' located at *7D* from the 180^O bend. The value of the pressure pulse (P_O) is not required however for computation when the inlet velocity is prescribed. The pressure-drop between the inlet and section G-G' obtained from the solutions of the Navier-Stokes equations is in good agreement with that due to acceleration calculated with $\rho L dV/dt$ = 5820 Pa or 43.65 mmHg (L being the tube length). The flow rate is kept unchanged thereafter for studying flow development at a Reynolds number **Re =** 1476. The 3D boundary layer and core flow are different from the pulsating flow in the aorta [10, 11] which is characterized by a time-dependent Reynolds number **Re**(t). Small pressure variations on the symmetric plane are shown in Figure 1 (b), (c) and (d) for *t = 0.24, 1.0s and 5.7s* are due to viscous resistance without changing the flow rate (*dV/dt* = 0). Higher pressures along the outer wall reflect the impact of centrifugal acceleration. It is noteworthy that in real clinical applications, the size and shape of the cross sections can also contribute to skewness and recirculation of the flow regardless of the radius of curvature of the blood vessel. Furthermore, the acceleration due to centrifugal forces can induce skewness in the flow towards the inner wall with associated recirculation at the inner wall. This can manifest in increased boundary layer thickness (hydrodynamic) at both the inner and outer walls as noted in Seed and Wood [12] and also Nerem *et al.* [13]. **Figures 2 and 3** depict the longitudinal velocity contours along the curve tube; they are varied with time and eventually assume the steady state. The first column portrays *w*-contours at t = *0.02s* from section $\phi = 23^O$ to sections at 45^O, 90^O, 135^O, 180^O and D-D' (one diameter D from $\phi = 180^O$), indicating boundary layer development is occurring along the tube. Higher velocities near the inner bend are practically irrotational due to acceleration, curvature and the onset of a thin boundary layer. Peak velocity at section $\phi = 180^O$ is slightly lower than that at 135^O due to the influence of downstream straight tube. Velocities at section D-D' remain almost axisymmetric, indicating that the upstream effect has not yet been impactful at this instant (t = *0.02s*). The first row in Figure 2 shows velocity distribution contours at section $\phi = 23^O$ varying with time. The flow becomes fully developed at t = *0.5s*; that is no changes are computed in the flow structure thereafter. A similar development is noticeable at section $\phi = 45^O$ when $t = 1.0\ s$. The growth of the 3D boundary layer structure is dominated by higher momentum moving from the inner curved wall towards the outer bend under centrifugal pressures. The flow field from $\phi = 23^O$ to $\phi = 45^O$ forms a core (refer to w = 15 cm/s and 15.7 cm/s) in the entrance region. The dome-shaped w-contours at $\phi = 135^O$ and $t = 0.5s$ in Figure 3 are due to rapid elevation of the boundary layer along the inner bend with twin peaks computed in the southeast and southwest regions in the 3D flow development. The dashed line in the contour plots at section $\phi = 180^O$ signifies a small back flow in the zone of separation although the effect is not significant on the transient processes. The bowtie *w*-contours are associated with a pair of secondary vortices which are characteristic of curved tube hydrodynamics (Dean counter-rotating vortices)- see Figure 5. Further viscous flow development from $t = 0.5s$ *to* $1.0s$ is also observed in columns 3 and 4. The circular core at section $\phi = 45^O$ is enlarged at $t = 1.0s$. The mushroom shaped *w*-contours appear along the inner bend at sections $\phi = 135^O$, 180^O and D-D'. They are associated with secondary flows resulting in the transfer of greater momentum toward the outer wall. Scrutiny of the *w*-contours in the first row of Figure 2, shows the velocity distribution at section $\phi = 23^O$ and 45^O becoming fully established, respectively, at $t = 0.5s$ *and* $1.0s$. Velocity contours in column 5 of Figures 2 and 3 become steady from the inlet to section $\phi = 180^O$ at $t = 2.3s$. However, the 3D boundary layer continues to develop in the downstream and may exhibit thickening. The computation was prolonged to *6.9s* to approach the steady state.

Flow development in the straight tube downstream is visualized in **Figure 4**. Rows 1, 2 and 3 of the first three columns depict velocity contours on E-E', F-F' and G-G' sections at *3D, 5D and 7D* from the 180^O bend, respectively. Longitudinal velocity distributions in the first column become axisymmetric from section F-F'. Velocities at F-F' and G-G' sections are approximately the same along with the growing boundary layer. The *w*-contours in columns 2 and 3 indicate that higher momenta are generated in the flow near the outer wall moving back towards the central region from section $\phi = 180^O$ to the downstream sections. The results show the 3D flow evolution from the curved segment toward axisymmetric flow in the downstream. The kinematic, dynamic and energy characteristics of the 3D flow development are correlated in **Figure 5**. The first column shows secondary flow patterns at sections $\phi = 45^O$, 90^O, 135^O and 180^O. The second column presents longitudinal velocity (*w*-contour) along with secondary flow patterns (as dashed lines). They are paired with the pressure contours in column 3. Since the computational analysis is based on a constant pressure P_O at section G-G', no radial pressure gradient appears there. The fourth column gives the total head (*H*) expressed as ρgH in Pascal. The velocity head is dominated by the longitudinal velocity component (*w*). The total head contour is produced due to pressure and longitudinal momentum. The difference between columns 4 and 5 indicates the kinetic energy. Due to the symmetrical plane, one can visualize a pair of clockwise and counterclockwise 3D spiral streamlines formed along the curve tube, portraying the complexity of the boundary layer development with the core flow. The spiral flow structure contributes also to boundary layer growth, secondary velocities and also recirculation regions. It is extremely complex in real hemodynamics and interacts extensively with the boundary layer structure.

The rapid development of the 3D flow processes is summarized by comparing longitudinal velocity distribution from the inlet to the outlet as shown in **Figure 6**. High momentum on the inner bend at $t = 0.02s$ is attributable to the curvature and the impulsive flow acceleration. The rapid growth of the boundary layer with time and along the inner bend is demonstrated at $t = 0.24s$. Peak velocities by the inner bend continue to migrate from the inner bend toward the outer wall (see $t = 1.0s$). Comparison of w-contours between this time and at $t = 2.3s$ indicates that the boundary layer and the main flow are well balanced and developed from the inlet to $\phi = 180^o$. This would imply that viscous forces are balanced by inertial and centrifugal forces and separation is not generated at the inner wall. However, higher momenta zones near the outer wall are progressively displaced back towards the central region of the straight tube. Velocity distributions approach the classical Hagen-Poiseuille flow in the downstream.

4.Conclusions

A numerical investigation of the blood flow in a curved tube geometry has been conducted using a finite volume approach. The computational analysis has successfully captured the 3D boundary layer development with core flow along the curve tube. Using a sudden acceleration to obtain flow kinematics and dynamics provides a realistic initial condition for computation [8]. Directly seeking steady flow solutions from the Navier-Stokes equations could encounter numerical instability due to initially assumed velocity distribution and nonlinear convective acceleration[14]. The 3D flow processes are presented in detail via longitudinal velocity contours across various sections. The entrance region is dominated by uniform velocity at the inlet and the centrifugal forces. Large pressure drop at the onset flow is due to the strong acceleration comparable to generating systolic pressures. A continued increase in flow rate is required to maintain the pressure wave in the aorta. The kinematic, dynamic and energy characteristics are correlated by secondary flow with longitudinal velocity contours, pressure distribution and the total head. Velocity distributions approach the Hagen-Poiseuille flow in the downstream straight tube. The spiral flow processes calculated and visualized by using CFD software reflect the usefulness of computational models for biomedical simulations and indeed are applicable to other areas of hydrodynamics including pipeline design. The present numerical methodology has been applied to Newtonian blood only. Future investigations may consider smaller blood vessels in which non-Newtonian effects become substantial and can be accommodated with a range of appropriate haemo-rheological formulations including micropolar[15], viscoelastic[16] and viscoplastic models[17]. Efforts in these directions are underway and will be reported imminently.

Acknowledgments

The fellowships from the Medical Device Innovation Centre of the National Cheng Kung University for Cheng-Hsien Chiang and Rui-Hung Kao to visit the University of Pittsburgh are acknowledged. The study is developed through the NCKU-Pitt initiative of Professor Fong-Chin Su of NCKU and Professor Tin-Kan Hung of the University of Pittsburgh.

References

1. Dean, W. R, The stream-line motion of fluid in a curved pipe, *Philosophy Maganzine*, **5**(30), 1928, 673-695.

2. Taylor, G. I, The criterion for turbulence in curved pipes, *Proc. Royal Society. Lond a-Conta* **24** (794), 1929, 243-249.

3. Barua, S. N, On secondary flow in stationary curved pipes, *Quart. J. Mechanics and Applied Mathematics*, **16**(1), 1963, 61-77.

4. Berger, S. A, Talbot, L, and Yao, L. S, Flow in curved pipes, *Annual Review of Fluid Mechanics*, **15**, 1983, 461-512.

5. Fry, D. L, Acute vascular endothelial changes associated with increased blood velocity gradients. *Circulation research*, **22**(2), 1968,165-197.

6. Hung, T. K, Cheng, W. S. Li, D. F, Guan, J. H, and Chen, B. F, Accelerated flows in rigid and distensible curved tubes. *Engineering Science - Fluid Dynamics: A Symposium To Honor T. Y. Wu*, World Scientific Publishing, 1989, 147-160.

7. Hung, T. K, Cheng, W. S, and Li, D. F, Pulsatory entry flow in a curbed tube, *Proceedings of Advancements in Aerodynamics, Fluid Mechanics and Hydraulics, ASCE Speciality Conference, Minneapolis, Minnesota, United States, June 3-6,*1986, 669-676.

8. Hung, T. K, Spiral Flows in finite rotating annular tubes, *ASCE Journal of the Engineering Mechanics Division*, **90**, ASCE, 1973, 13-29.

9. Hirt, C. W, Amsden, A. A, and Cook, J. L, An arbitrary Lagrangian-Eulerian computing method for all flow speeds, *Journal of Computational Physics*, **135**(2), 1974, 203-216.

10. Hung, T. K, Kuo, R. H, and Chiang, C. H, Kinematic and dynamic characteristics of pulsating flow in 180^{O} Tube, *MCB Molecular and Cellular Biomechanics*, **17**(1), 2020, 19-24.

11. Hung, T. K, Khalafvand, S. S, and Ng. E. Y. K, Fluid dynamic characteristics of systolic blood flow of the left ventricle, *J. of Mechanics in Medicine and Biology*, **15**, 2015, 1-20.

12. Seed, W. A., and Wood, N. B., Velocity patterns in the aorta, *Cardiovasc. Res*., **5**, 1971, 319–330.

13. Nerem, R. M., Seed, W. A., and Wood, N. B., An experimental study of the velocity distribution and transition to turbulence in the aorta, *J. Fluid Mech*. **52**, 1972, 137–160.

14. Macagno, E. O, Hung, T. K, Computational and experimental study of a captive annular eddy, *Journal of Fluid Mechanics*, 1967, **28**, (1), 43-64.

15. O. Anwar Bég, H.S. Takhar, R. Bhargava, S. Sharma and T-K Hung, Mathematical modeling of biomagnetic flow in a micropolar fluid-saturated Darcian porous medium, *Int. J. Fluid Mechanics Research*, 34, **5**, 403-424, 2007.

16. Nasir Ali, Akbar Zaman, O. Anwar Bég, M.Sajid, Unsteady two-layer blood flow through a *w*-shape stenosed artery using the generalized Oldroyd-B fluid model, *ANZIAM Journal*, **58**, 1-23, 2016.

17. Ashis Kumar Roy, Sudip Debnath and O. Anwar Bég, Transient solute dispersion in electro-osmotic viscoplastic flow in a microchannel, *ZAMM- J. Applied Mathematics and Mechanics* (2023). *DOI: 10.1002/zamm.202200260 (16 pages)*

Figures and Captions

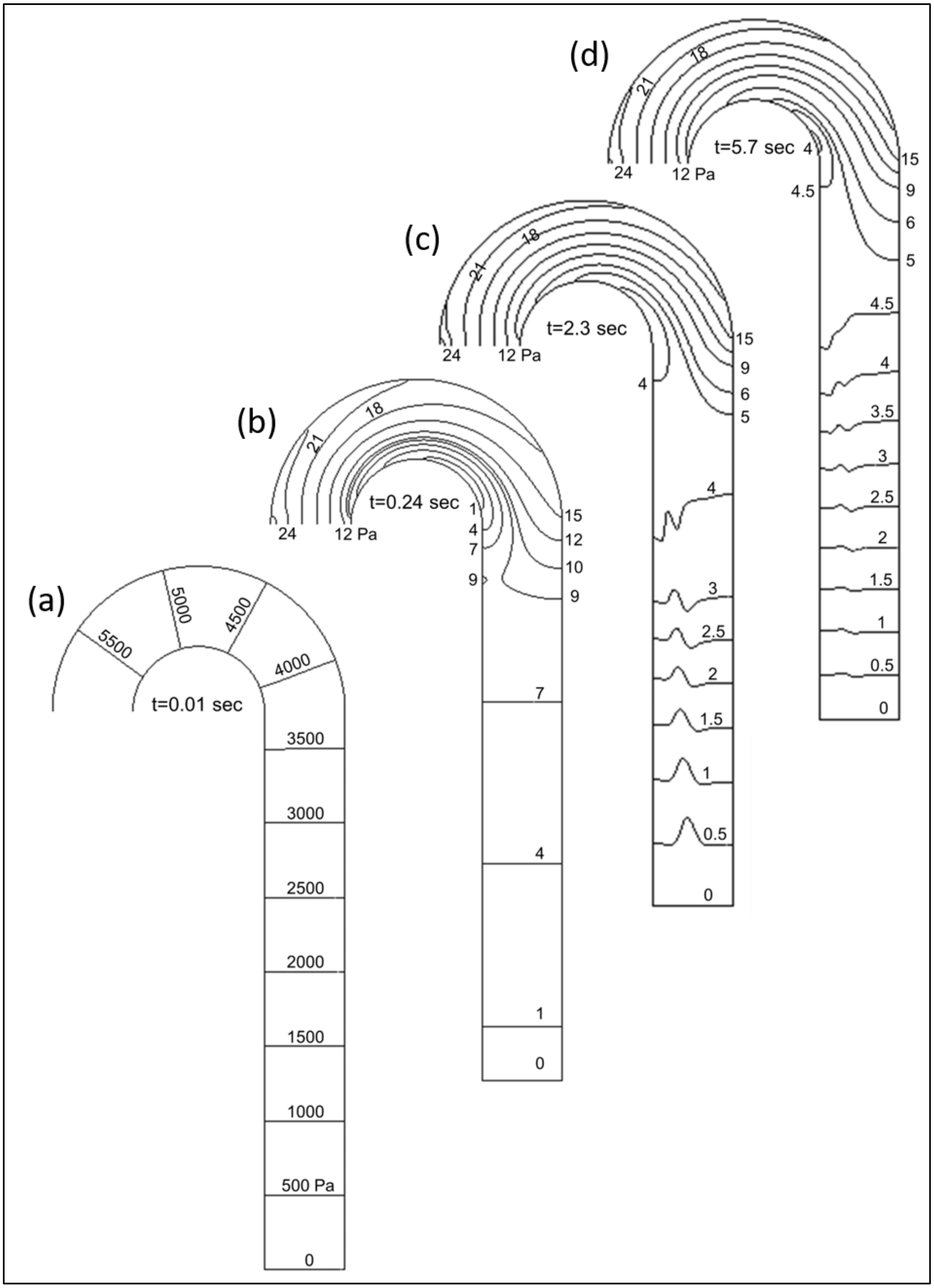

Figure 1. Pressure distributions on the symmetric plane for t = 0.01, 0.24, 2.3 and 5.7 second.

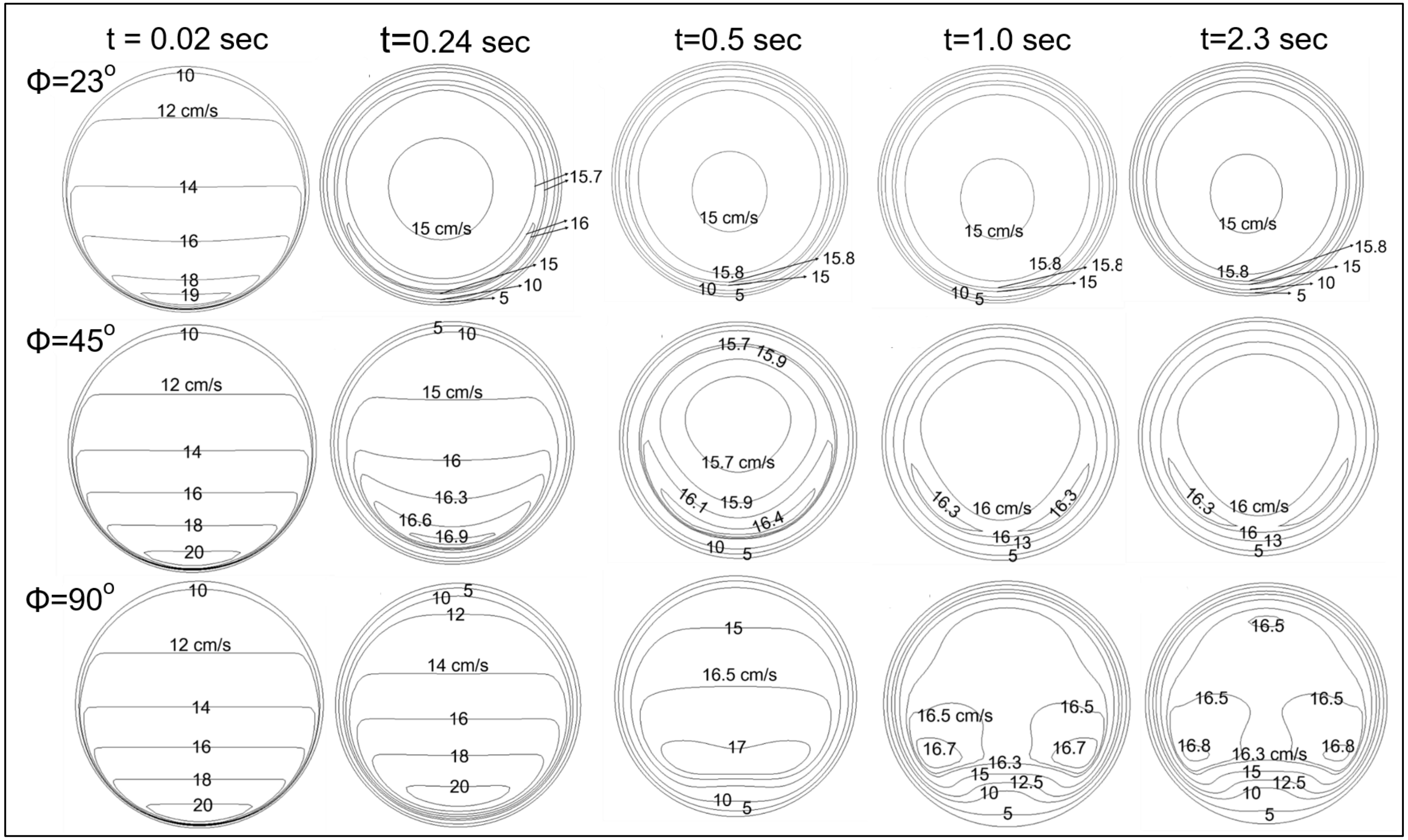

Figure 2. Development of longitudinal velocity along the curved tube from section ϕ = 23˚ to 45˚ and 90˚.

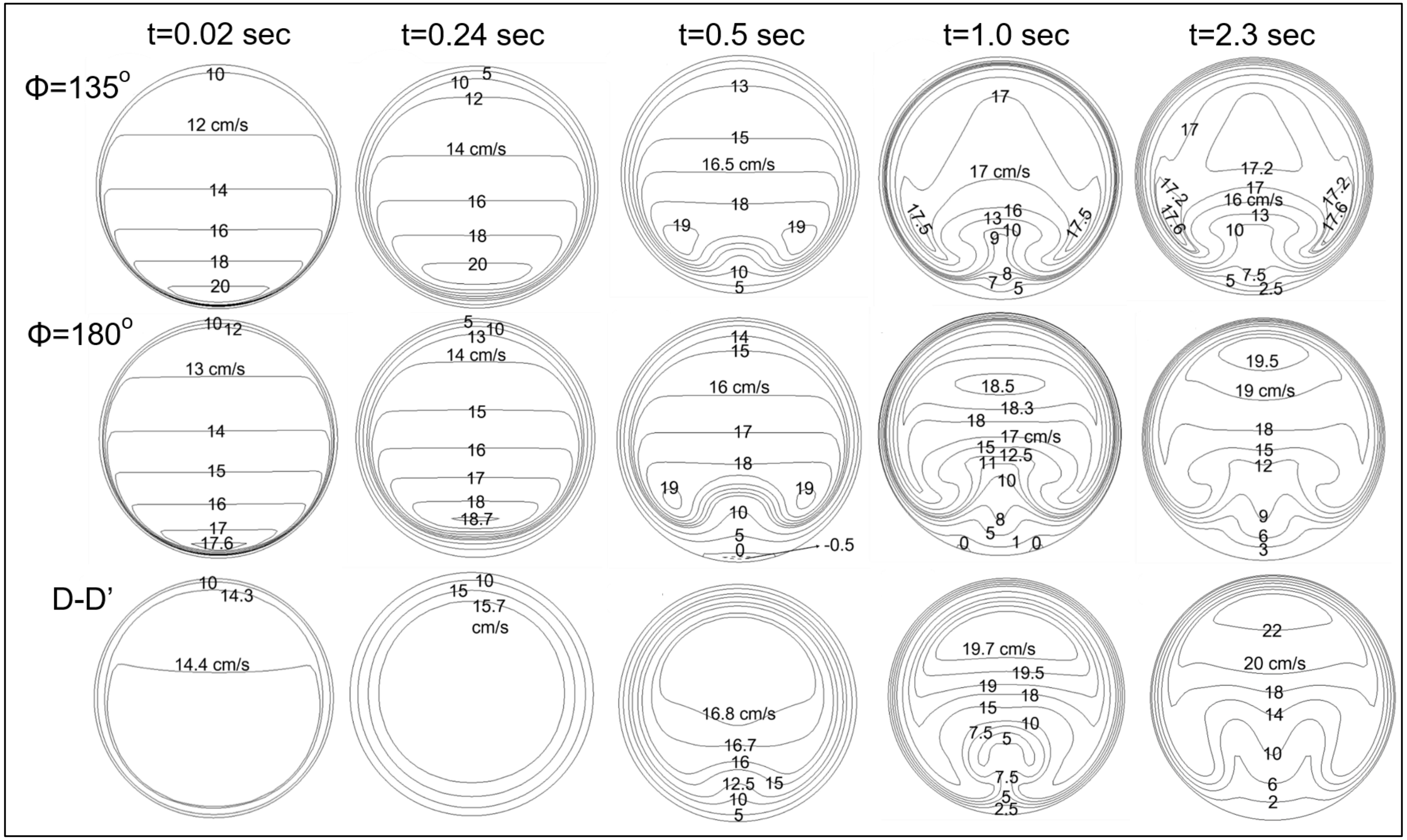

Figure 3. Development of longitudinal velocity along the curved tube from section $\phi = 135^\circ$ to 180° and D-D' section.

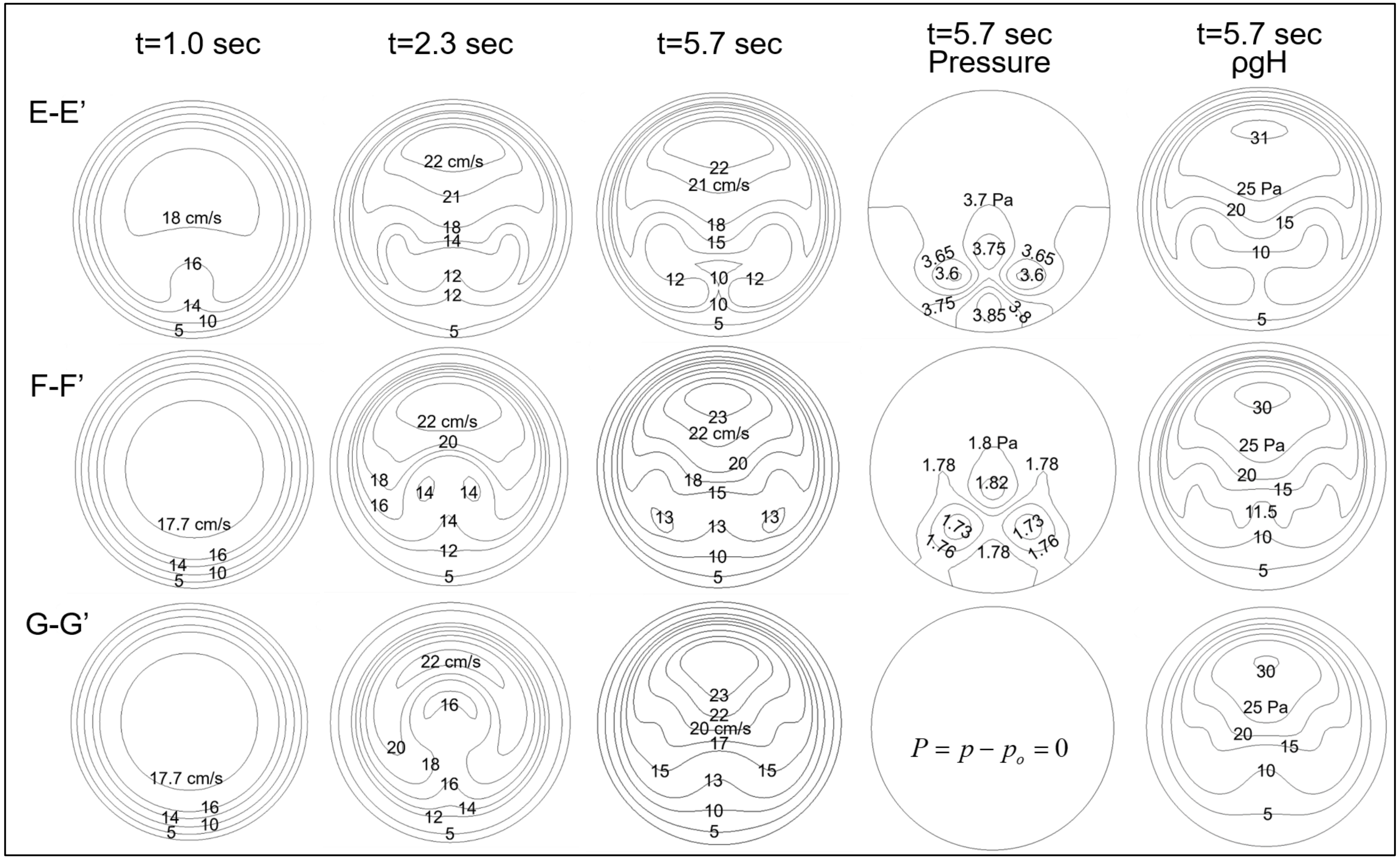

Figure 4. Development of longitudinal velocity, pressure contours and total head in the straight tube at sections E-E', F-F' and G-G'.

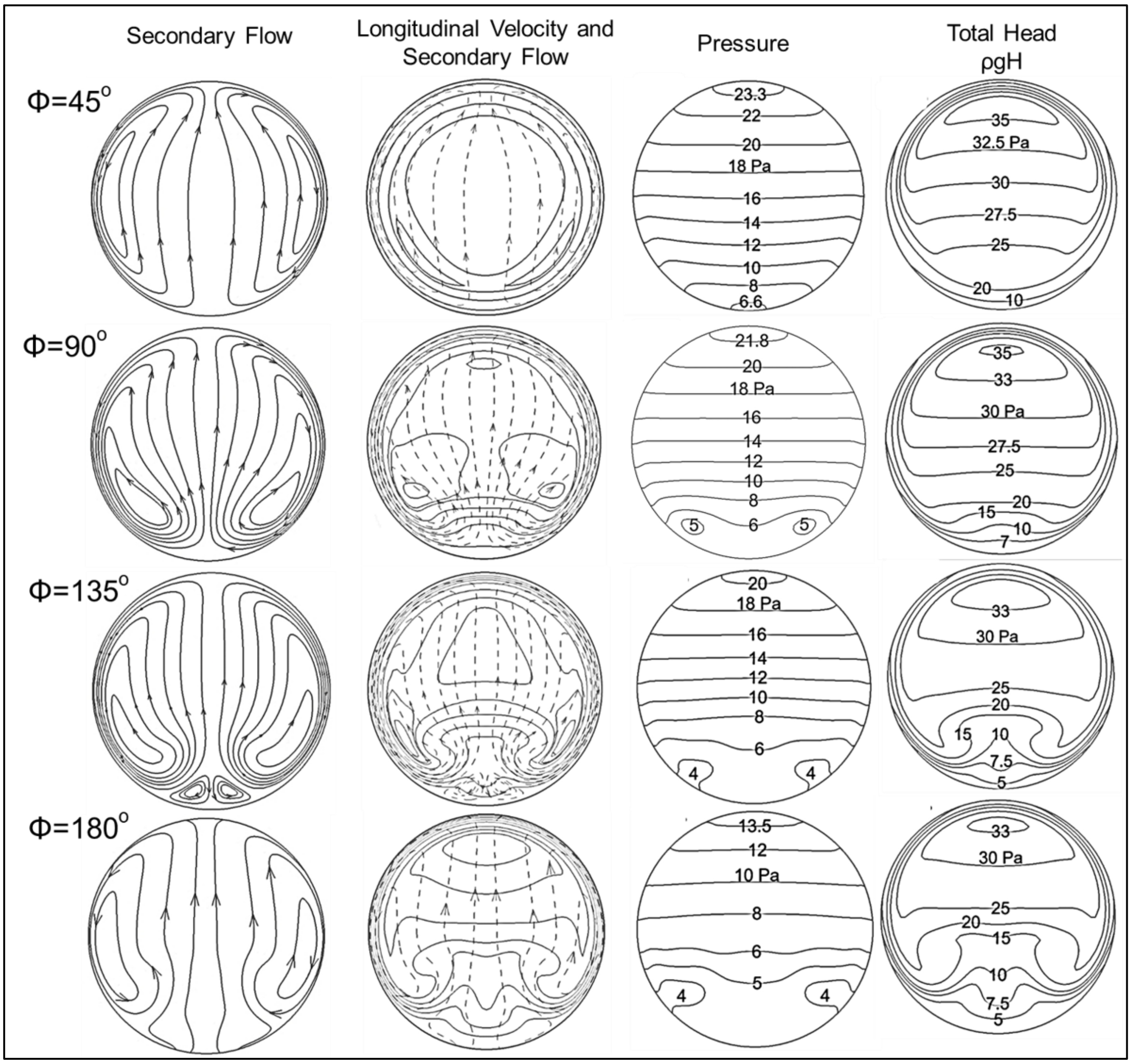

Figure 5. Secondary flow, longitudinal velocity contours and secondary flow, pressure contours and total head distribution contours.

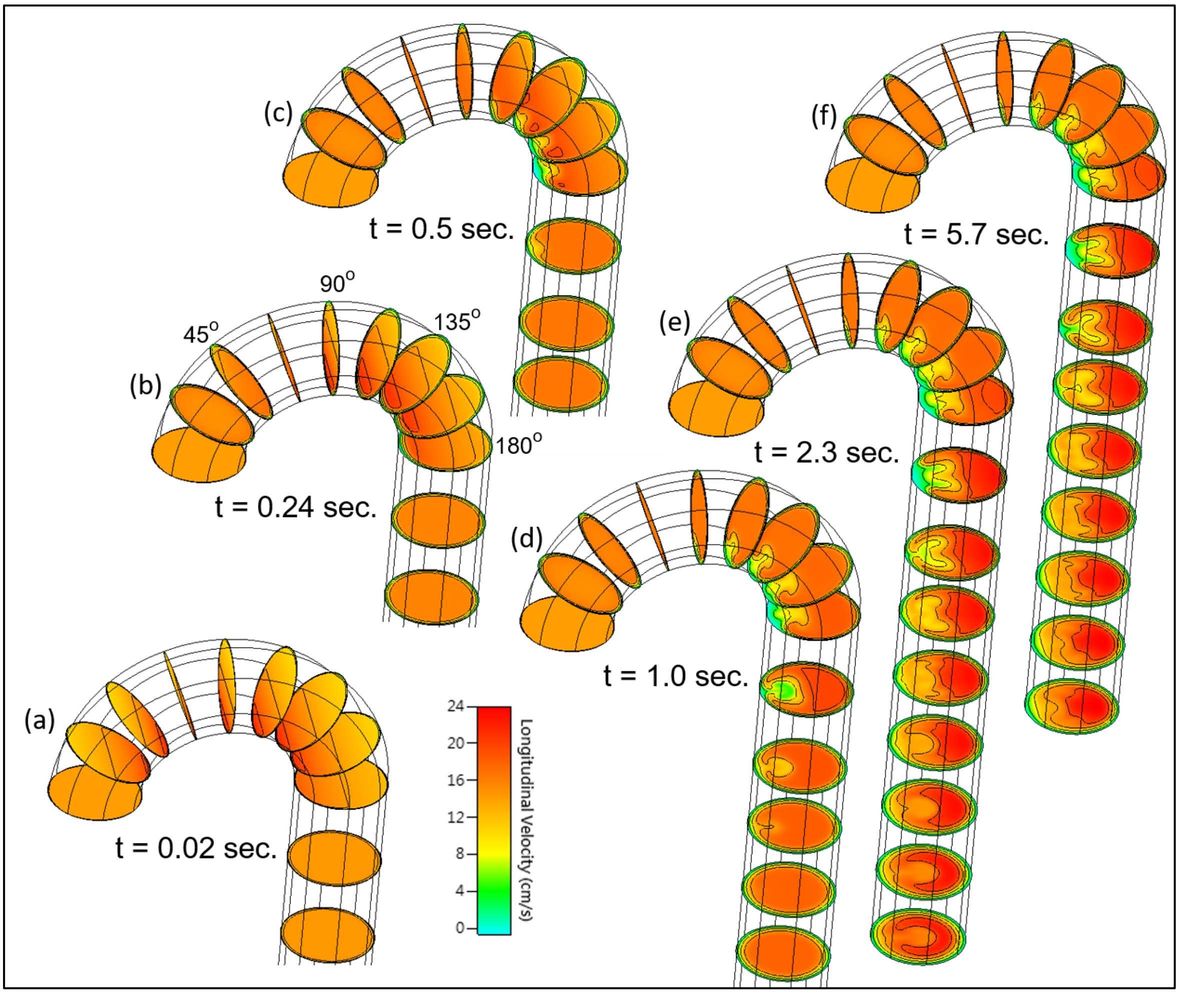

Figure 6. Three-dimensional visualization of longitudinal velocity distributions across various sections of the 180^{O} curved tube.